

## Aberystwyth University

### *Snow cover and snow albedo changes in the central Andes of Chile and Argentina from daily MODIS observations (2000-2016)*

Malmros, Jeppe K.; Mernild, Sebastian H.; Wilson, Ryan; Tagesson, Torbern; Fensholt, Rasmus

*Published in:*

Remote Sensing of Environment

*DOI:*

[10.1016/j.rse.2018.02.072](https://doi.org/10.1016/j.rse.2018.02.072)

*Publication date:*

2018

*Citation for published version (APA):*

Malmros, J. K., Mernild, S. H., Wilson, R., Tagesson, T., & Fensholt, R. (2018). Snow cover and snow albedo changes in the central Andes of Chile and Argentina from daily MODIS observations (2000-2016). *Remote Sensing of Environment*, 209, 240-252. <https://doi.org/10.1016/j.rse.2018.02.072>

#### **General rights**

Copyright and moral rights for the publications made accessible in the Aberystwyth Research Portal (the Institutional Repository) are retained by the authors and/or other copyright owners and it is a condition of accessing publications that users recognise and abide by the legal requirements associated with these rights.

- Users may download and print one copy of any publication from the Aberystwyth Research Portal for the purpose of private study or research.
- You may not further distribute the material or use it for any profit-making activity or commercial gain
- You may freely distribute the URL identifying the publication in the Aberystwyth Research Portal

#### **Take down policy**

If you believe that this document breaches copyright please contact us providing details, and we will remove access to the work immediately and investigate your claim.

tel: +44 1970 62 2400

email: [is@aber.ac.uk](mailto:is@aber.ac.uk)

1 **Snow cover and snow albedo changes in the central Andes of Chile and Argentina**  
2 **from daily MODIS observations (2000–2016)**

3  
4 JEPPE K. MALMROS,<sup>1</sup>, SEBASTIAN H. MERNILD,<sup>2,3,4</sup>, RYAN WILSON,<sup>5</sup>,  
5 TORBERN TAGESSON,<sup>1</sup>, RASMUS FENSHOLT,<sup>1</sup>

6  
7 <sup>1</sup> *Department of Geosciences and Natural Resource Management, University of Copenhagen,*  
8 *Copenhagen, DENMARK*

9  
10 <sup>2</sup> *Nansen Environmental and Remote Sensing Center, Bergen, NORWAY,*

11  
12 <sup>3</sup> *Direction of Antarctic and Sub-Antarctic Programs, Universidad de Magallanes, Punta Arenas,*  
13 *CHILE*

14  
15 <sup>4</sup> *Faculty of Engineering and Science, Western Norway University of Applied Sciences, Sogndal,*  
16 *NORWAY*

17 <sup>5</sup> *Department of Geography and Earth Sciences, Aberystwyth University, Aberystwyth, UK*

18  
19  
20  
21  
22 *Resubmitted to Remote Sensing of Environment February 22nd, 2018*

23  
24  
25  
26  
27  
28  
29 Corresponding author address:

30 Department of Geosciences and Natural Resource Management, University of Copenhagen, Øster  
31 Voldgade 10, 1350 Copenhagen, Denmark.

32 E-mail: jkmalmros@gmail.com

33 **Abstract**

34           The variables of snow cover extent (SCE), snow cover duration (SCD), and snow albedo (SAL)  
35 are primary factors determining the surface energy balance and hydrological response of the  
36 cryosphere, influencing snow pack and glacier mass-balance, melt, and runoff conditions. This study  
37 examines spatiotemporal patterns and trends in SCE, SCD, and SAL (2000–2016; 16 years) for central  
38 Chilean and Argentinean Andes using the MODIS MOD10A1 C6 daily snow product. Observed  
39 changes in these variables are analyzed in relation to climatic variability by using ground truth  
40 observations (meteorological data from the El Yeso Embalse and Valle Nevado weather stations) and  
41 the Multivariate El Niño index (MEI) data. We identified significant downward trends in both SCE and  
42 SAL, especially during the onset and offset of snow seasons. SCE and SAL showed high inter-annual  
43 variability which correlate significantly with MEI applied with a one-month time-lag. SCE and SCD  
44 decreased by an average of  $\sim 13 \pm 2 \%$  and  $43 \pm 20$  days respectively, over the study period. Analysis of  
45 spatial pattern of SCE indicates a slightly greater reduction on the eastern side ( $\sim 14 \pm 2 \%$ ) of the  
46 Andes Cordillera compared to the western side ( $\sim 12 \pm 3 \%$ ). The downward SCE, SAL, and SCD  
47 trends identified in this study are likely to have adverse impacts on downstream water resource  
48 availability to agricultural and densely populated regions in central Chile and Argentina.

49  
50  
51  
52  
53  
54  
55  
56  
57  
58  
59  
60

61 **Keywords:** Andes; Argentina; Chile; climate change; ENSO; MOD10A1; MODIS; snow albedo; snow  
62 cover extent; time series analysis.

## 63 **1. Introduction**

64 Snow in the semi-arid mountain regions of the central Andes of Chile and Argentina provides  
65 important water resources to more than 10 million people and is of major importance for agriculture in  
66 this area (Masiokas et al. 2006). Moreover, snow constitutes a key seasonal component in the surface  
67 energy and hydrosphere budgets, reflecting incoming solar shortwave radiation (e.g., Konzelmann and  
68 Ohmura 1995). Hydrological balance in the cryosphere is highly influenced by the amount of snow  
69 precipitation and the spatiotemporal variability of seasonal snow cover extent (SCE). The combined  
70 variability of snow precipitation, SCE, and snow cover duration (SCD) directly influences river-runoff  
71 variabilities and glacier surface-mass balance conditions (Ragettli et al. 2016; Wilson et al. 2016).

72 On high mountain glaciers, energy availability for snow and ice melt is regulated by surface  
73 albedo which is defined as the ratio of incoming solar radiation reflected by a surface (Cuffey and  
74 Paterson 2010). Fresh snow, for example, acts as a near perfect reflector with albedo values of up to  
75 0.98. However, snow albedo (SAL) diminishes over time as a result of snow metamorphism,  
76 decreasing to as low as 0.46 (Cuffey and Paterson 2010). Rainfall can further enhance this natural  
77 lowering of SAL through the addition of latent energy, which can initiate melting (Benn and Evans  
78 2010) and cause downwasting and thinning of glaciers (Neckel et al. 2017). Snow and ice albedo can  
79 also be reduced by the surface deposition of dust and/or anthropogenic soot (Hansen and Nazarenko  
80 2004; Cereceda-Balic et al. 2012). In the central Andes, an additional factor which influences SAL is  
81 the seasonal formation of penitents. Often forming in areas of low humidity and high solar elevation,  
82 snow penitents can result in significant changes in the surface roughness of snow-covered terrain,  
83 which, in turn, influences SAL and sublimation conditions (Corripio and Purves 2006).

84 The overall variability of SAL is influenced by a variety of factors: snow grain size, levels of  
85 contamination, solar zenith angle, cloud cover, snow metamorphism, surface roughness, age factor, and  
86 liquid water content, amongst others (Warren and Wiscombe 1980; Mernild et al. 2015a). Since SAL is  
87 a key parameter determining the amount of energy available for surface melting snow and ice, snow-  
88 sublimation, and metamorphosis, spatiotemporal variability in SAL is important when determining  
89 snow ablation conditions (Male and Granger 1981; Brock et al. 2000; Hock 2005; Gardner and Sharp  
90 2010; Mernild et al. 2016a).

91 Spatiotemporal trends in SCE and SAL interpolated from point measurements often include  
92 large errors, especially in remote mountainous regions characterized by limited ground observations,

93 localized climate conditions and complex terrain. In comparison, satellite-based remote sensing and  
94 satellite derived snow cover products provide opportune sources of large-scale SCE and SAL  
95 measurements and have been successfully used as key inputs in climate, atmospheric and hydrological  
96 models (Farr et al. 2007; Mernild et al. 2008; Vuille et al. 2008; Mernild et al. 2015a). Remote sensing  
97 systems acquiring data from the visible (VIS) to shortwave infrared (SWIR) spectrum with a high  
98 temporal resolution are well suited for monitoring SCE and SAL over large areas, providing good  
99 spatial and temporal coverage (Wiscombe and Warren 1980; Dozier and Frew 1981; Dubayah 1992;  
100 Knap et al. 1999).

101 Several remote sensing based snow cover products are currently available, most of which apply  
102 either the normalized difference snow index (NDSI) (Hall et al. 1995), empirical relationship  
103 assumptions or spectral un-mixing models (Klein and Stroeve 2002a). Optical sensor systems,  
104 however, are unable to acquire useful information during cloudy conditions (Justice et al. 1998;  
105 Marchane et al. 2015). Therefore, frequent satellite observation revisits are essential to study changes  
106 in SCE and SAL, since surface conditions can vary rapidly and may change considerably over a few  
107 days.

108 To compensate for extensive cloud cover, compromises are often made by conducting satellite  
109 analysis based on composite products such as the MODIS (Moderate Resolution Imaging  
110 Spectroradiometer) 8 day snow cover MOD10A2 product (Hall et al. 2002), which can mask subtle  
111 changes in SCE and SAL over time. In order to avoid this limitation, the MODIS MOD10A1  
112 Collection 6 (C6) dataset was used this study. MOD10A1 provides daily SCE and SAL values globally  
113 at a spatial resolution of 500 m, making it suitable for evaluating seasonal trends in SCE and SAL (Hall  
114 et al. 2002; Liang et al. 2005; Marchane et al. 2015; Hall and Riggs 2016; Saavedra et al. 2016; Li et al.  
115 2017; Huang et al. 2017; Dariane et al. 2017), snow cover phenology (Xu et al. 2017) and the relation  
116 between SCE and climate (Gurung et al. 2017; Li et al. 2017). Using MOD10A1 data, this study  
117 analyses spatiotemporal changes in SCE and SAL in the central Andes of Chile and Argentina by  
118 parameterizing a time series of seasonal SCE and SAL metrics at the per-pixel level. Furthermore, this  
119 study examines the large-scale influence of ENSO events on SCE and SAL as well as the more  
120 localized effect of climatic variability (utilizing meteorological data from the El Yeso Embalse (EYE)  
121 and Valle Nevado (VN) automatic weather stations (AWS)) and elevation.  
122

123 **2. Study area**

124 The Andes of central Chile and Argentina (31°S and 40°S) contain some of the highest peaks of  
125 the entire Andes Cordillera, reaching altitudes above 6,000 m above sea level (a.s.l.) (Fig. 1). Covering  
126 an area of ~1,730 km<sup>2</sup>, the study area chosen is located immediately west of Santiago de Chile  
127 (32°50'– 34°50'S; 69°20' – 70°40'W). This study area includes several river basins which supply  
128 freshwater to large downstream populations (10+ million people in Chile and 2+ million in Argentina),  
129 hydro-power stations, and agricultural lands on both sides of the cordillera (Corripio and Purves 2006).  
130 This area of the central Andes also includes the largest glaciated areas in South America outside  
131 southern Patagonia (Saavedra et al. 2016). River runoff in this central region originates primarily from  
132 snowmelt (Masiokas et al. 2006), with snowfall contributing up to ~85 % of runoff from specific  
133 catchments (Mernild et al. 2016b). The availability of snow as a freshwater resource is therefore of  
134 vital socio-economic importance in this semi dry region (Peña and Nazarala 1987; Meza et al. 2012;  
135 Carey et al. 2017).

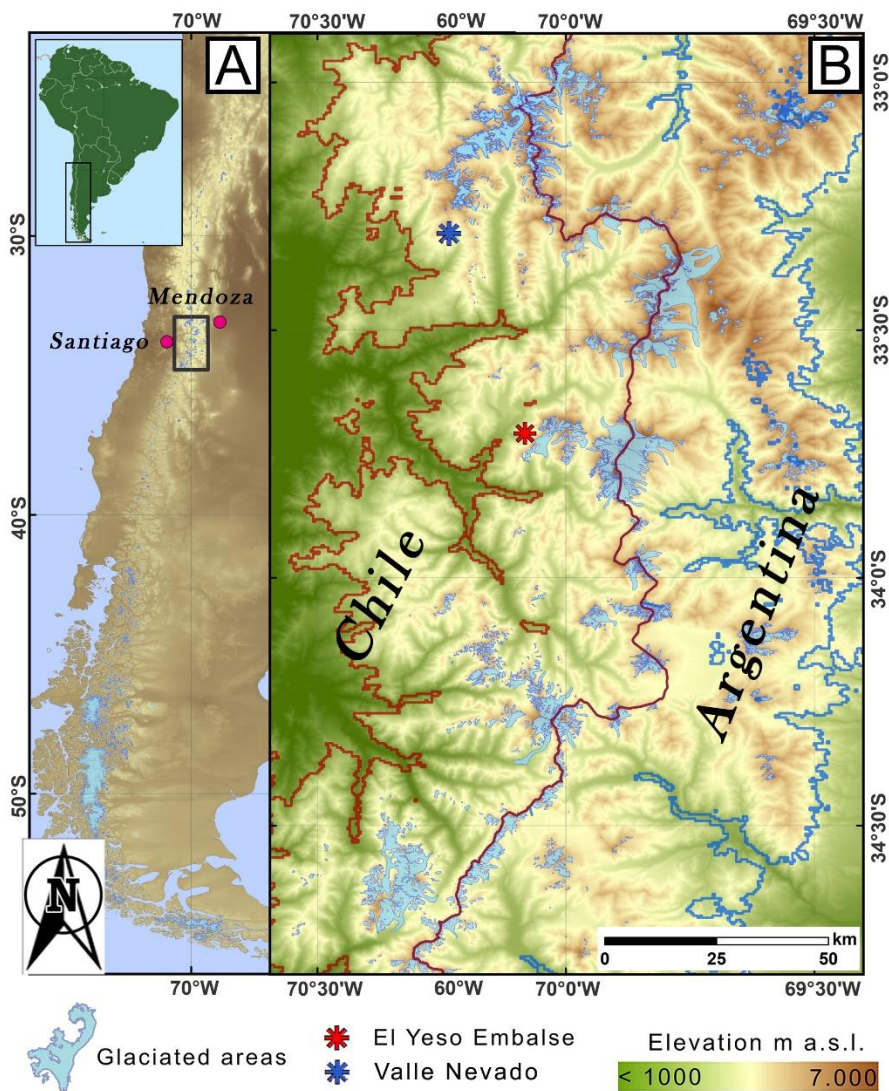
136 The intra-annual variability of precipitation in central Andes is highly influenced by the  
137 placement of an atmospheric high-pressure cell over the southeastern Pacific Ocean. This cell normally  
138 inhibits precipitation in the Austral summer (December – February) and allows for the passage of  
139 westerlies and frontal precipitation during Austral winters (June – August) (Garreaud et al. 2009).  
140 Precipitation events are usually concentrated between April and October, providing ~95 % of the mean  
141 annual totals, peaking in June or July (Masiokas et al. 2016). The strength of El Niño Southern  
142 Oscillation (ENSO) influences inter-annual variability in precipitation, with higher/lower precipitation  
143 occurring during El Niño/La Niña events (Rutllant and Fuenzalida 1991; Escobar et al. 1995; Leiva  
144 1999; Montecinos and Aceituno 2003; Garreaud et al. 2009). During El Niño events, precipitation  
145 increases predominantly during the austral winter (Masiokas et al. 2006; McClung 2013). Whilst El  
146 Niño events do influence precipitation amounts, these events shows little or no significant signal in  
147 annual mass balance measurements of glaciers located in the central Andes but has been linked to the  
148 Pacific Decadal Oscillation (PDO) rather than the ENSO (Mernild et al. 2015a).

149 Along the central Andes, annual accumulation of snow is highest at 4,000 – 5,000 m a.s.l.,  
150 where glacier accumulation zones are also present (Cornwell et al. 2016; Mernild et al. 2016b; Mernild  
151 et al. 2016c). Precipitation differences observed between the western and eastern sides of the Andes  
152 Cordillera occur due to the combination of orographic effects of the mountain relief and the dominating

153 westerly wind direction which results in precipitation amounts and humidity being lower on the eastern  
154 Cordillera slopes (Cornwell et al. 2016; Mernild et al. 2016b).

155 For the central Andes, mean surface air temperatures are normally highest between December  
156 and March and lowest in July and August (Masiokas et al. 2016) and temperatures in the Andes showed  
157 increasing trends from 1975 to 2006 ( $\square 0.25^{\circ}\text{C}/\text{decade}$ ) (Falvey and Garreaud 2009). The  $0^{\circ}\text{C}$  isotherm  
158 for the western side of the cordillera (40 km northeast of Santiago de Chile), was located at 3,385 m  
159 a.s.l. between 2009 and 2014 (Mernild et al. 2016c).

160



161

162 Figure 1: (a) The central Andes of Chile and Argentina; and (b) including the area of interest west and  
163 east snow cover regions delineated by red and blue lines, respectively. The divide between the western

164 and eastern Andes also represents the natural border (continental divide) between Chile and Argentina.  
165 Blue areas represents glaciers. The red star in the center of the study area represents the location of the  
166 El Yeso Embalse (EYE) meteorological station (2475 m a.s.l.) and the blue star the Valle Nevado (VN)  
167 meteorological station (3050 m a.s.l.).

168

### 169 **3. Data**

170

#### 171 *3.1 MODIS data*

172 The MOD10A1 C6 (henceforth MOD10A1 unless other version is implied) snow product is  
173 derived from daily data acquisitions by the MODIS sensor aboard the Terra spacecraft (Riggs et al.  
174 2017). The MODIS global daily snow cover product MOD10A1 (MODIS/Terra Snow Cover Daily L3  
175 Global 500m Grid) is derived from cloud free observations and is well suited for regional snow cover  
176 and albedo mapping (Hall et al. 2002; Liang et al. 2005; Dozier et al. 2008; Rittger et al. 2013; Fausto  
177 et al. 2015; Mernild et al. 2015b). The latest MOD10A1 product was released in the spring of 2016 and  
178 includes a range of improvements to the previous version including, amongst others, the removal of  
179 Terra sensor degradation issues and improvements in atmospheric calibration (Lyapustin et al. 2014).  
180 Importantly, the algorithms used to compile the MOD10A1 snow product are modified to include only  
181 the best quality observations from the atmospherically corrected MOD10GA product (Hall et al. 2002).  
182 Individual MOD10A1 product parts include NDSI, NDSI snow cover (SCE), SAL and corresponding  
183 quality control flags. The MOD10A1 NDSI SCE is produced by using an empirical relationship with  
184 NDSI values, where NDSI values are multiplied by a constant (Dozier et al. 2008; Hall and Riggs  
185 2016). By using only full snow cover pixels, the accuracy of the MOD10A1 SAL product is improved  
186 in terms of ground truth comparisons (Sorman et al. 2007; Mernild et al. 2015b). The overall error of  
187 the MOD10A1 SAL product can vary substantially but is in the order of 1–10 % for good observations  
188 with low atmospheric disturbances across the Greenland ice sheet (Klein and Stroeve 2002b). The  
189 overall error at this location is likely higher due to the complex terrain of the Andes Mountains.  
190 However, changes in albedo can still be quantified and here we opted for a per-pixel temporal change  
191 analysis that is expected to mitigate the influence of topography to some degree by avoiding direct  
192 inter-comparison of pixels influenced by different slope/aspect.



193 MOD10A1 data used in this study was obtained from the NASA Earth Observation System  
194 Data and Information System (EOSDIS) Reverb ECHO website (<https://reverb.echo.nasa.gov/>). Out of  
195 the 5,844 potential scenes available between March 1 2000 and Feb 29 2016, only 121 (~2 %) were  
196 missing in the archive, with a maximum temporal gap of 17 days. The snow cover year (season) was  
197 set to start 1 March and end February 28 (29) based on analysis of the data set. Pixels with cloud cover  
198 or poor retrievals were omitted as determined from QA flags and only pixels flagged as “best quality”  
199 were included in the further analysis (see section 4.1). Out of all pixels in the data series 74.8 %  
200 contained “best quality” data (supplementary material S1).

201

202

### 203 *3.2 Ancillary data*

204 Elevation data were obtained from the Shuttle Radar Topography Mission (SRTM) v.3. SRTM  
205 provides elevation data at a spatial resolution of 30 meters with an overall vertical accuracy of ~10 m  
206 and geo-position error of ~9 m (Farr et al. 2007). Multivariate El Niño index (MEI) ranks were  
207 obtained from the National Oceanic and Atmospheric Administration (NOAA) website  
208 (<http://www.esrl.noaa.gov/psd/enso/mei/table.html>). The MEI provides a ranked index of the strength  
209 of El Niño and La Nina events. MEI values are normalized for each bimonthly season (Wolter and  
210 Timlin 2011) and cover the 16-year study period of snow cover and snow albedo observations.

211 We acquired mean monthly air temperature (MMAT), mean annual air temperature (MAAT),  
212 and monthly precipitation sums (2000–2016) from the El Yeso Embalse meteorological station (EYE)  
213 supported by available data from the Valle Nevado (VN) meteorological station from 2013 onwards  
214 (locations in Fig. 1; data shown in supplementary material S2 and S3) from Dirección General de  
215 Aguas (DGA; [www.dga.cl](http://www.dga.cl)) and CryoNET respectively  
216 (<http://globalcryospherewatch.org/cryonet/sitepage.php?surveyid=68>). Finally, glacier outlines were  
217 obtained from the Randolph glacier inventory v. 5.0 (Pfeffer et al. 2014) in combination with updated  
218 glacier shapes from 2013/2014 (Malmros et al. 2016).

219

## 220 **4. Methods**

221

### 222 *4.1 Time series preprocessing*

223 The MOD10A1 time series was preprocessed and analyzed using the program TIMESAT  
 224 (Jönsson and Eklundh 2002, 2004; Eklundh and Jönsson 2015). TIMESAT originally developed to  
 225 analyze vegetation seasonality can be applied to all remote sensing data containing seasonal variability.  
 226 We applied a Savitzky-Golay filter within TIMESAT to smooth the MOD10A1 time-series by applying  
 227 polynomial fitting to the data points within a moving window of a certain width (Savitzky and Golay  
 228 1964; Jönsson and Eklundh 2004). Missing dates were filled with blank scenes before smoothing  
 229 (Jönsson and Eklundh 2002) in order to compose a complete time series. Pixels not flagged as “best  
 230 quality” from the MOD10A1 QA flags were excluded from the analysis. The width of the moving  
 231 window influences the degree of smoothing and the ability of the filter to cope with rapid changes  
 232 (parameters used in the TIMESAT preprocessing are shown in Table 1). The polynomial fitting was  
 233 iterated and adapted to the upper part of the curve by assigning weights to data points above and below  
 234 the result of the previous step (Jönsson and Eklundh 2004). SCD was extracted in TIMESAT for SCE,  
 235 and the seasonal snow cover integral (SCI) (defined as the integral under the curve between onset and  
 236 end of seasonal snow cover) was extracted to evaluate the accumulated seasonal SCE for each season.  
 237 Areas characterized by limited seasonal variability were masked out due to the inability of the  
 238 TIMESAT algorithm to estimate SCD for such conditions. The mask was created from the median of  
 239 the 16 seasons and excluded areas with less than 16 days in the SCD dataset. Most excluded areas were  
 240 located in glacier accumulation zones where constant snow cover prevents seasonal variability in SCE.

241

242 Table 1: Input parameters for use in TIMESAT.

Parameter	NDSI Snow Cover	Snow Albedo
Seasonal parameter	0.7	0.7
Number of envelope iterations	3	3
Adaptation strength	2	2
Savitzky-Golay window size	15	15
Spike Method	Median filter	Median filter
Amplitude season start (%)	70	65
Amplitude season end (%)	20	46

243

244 *4.2 Trend estimation*

245 We conducted linear temporal trend analysis to estimate the magnitude and direction of changes  
246 in SCE, SAL, SCD, SCI, MAAT, and annual precipitation. We calculated per-pixel trends by applying  
247 a nonparametric linear regression model with time as the independent variable and the abovementioned  
248 variables as dependent variables. Since time series of the variables analyzed often do not meet  
249 parametric assumptions of normality and homoscedasticity, a median trend (Theil–Sen, TS) procedure  
250 was applied using the Theil–Sen slope estimator (median trend) which has proven robust against  
251 outliers (Eastman 2009). Uncertainty estimates of trends are calculated from standard deviations of the  
252 calculated metrics and are provided as  $\pm$  values to all trends reported. The significance of the trends  
253 was determined using the nonparametric Mann–Kendall test of significance (Mann 1945; Kendall  
254 1975). The Mann–Kendall significance test is commonly used as a trend test for the TS median slope  
255 operator (Eastman 2009) and produces outputs of z-scores that allow for the assessment of both the  
256 significance and direction of trends. The trends were considered significant at  $p < 0.05$  (where  $p$   
257 denotes the probability that there is no significant difference between observations over time). Trends  
258 in SCE, SCD, and SCI were extracted from the area of maximum values (minimum of 75% at any  
259 given time) for the entire study period and similar for SAL.

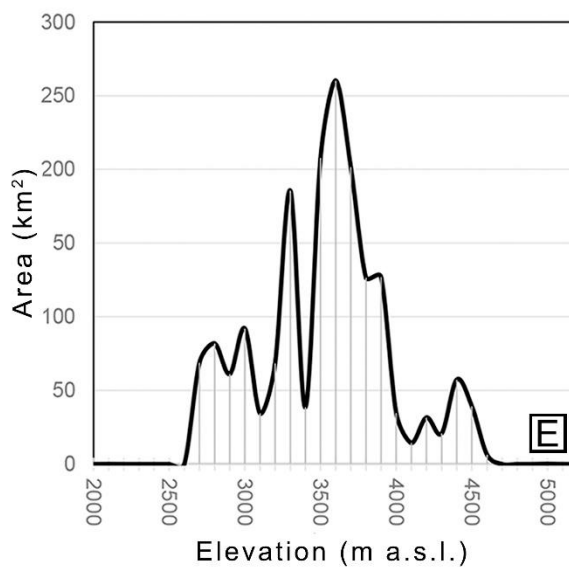
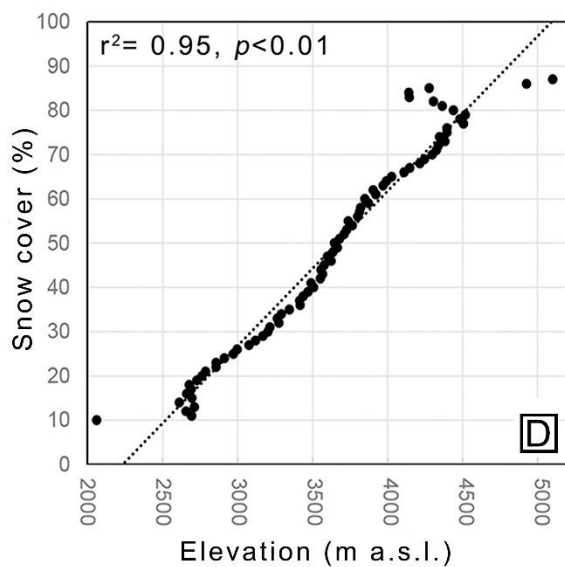
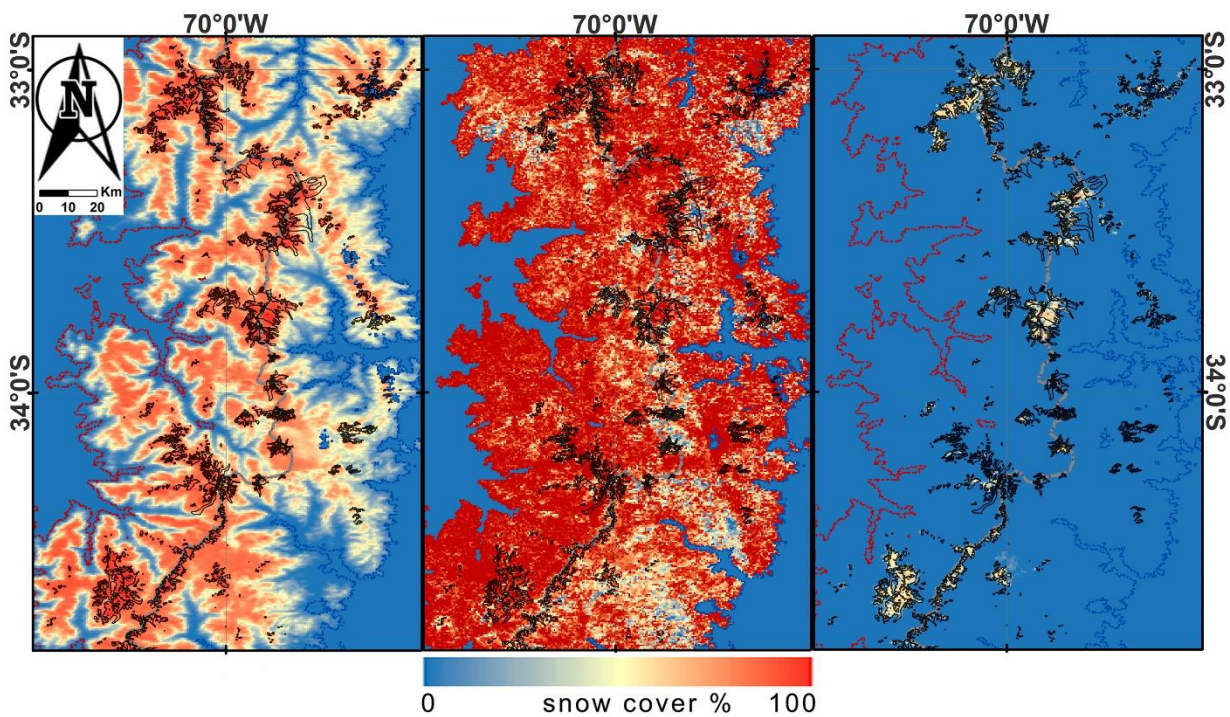
260

## 261 **5. Results**

### 262 *5.1 Spatio-temporal patterns in snow cover extent*

263 Statistical analysis of the MODIS time series revealed that the minimum, median, and  
264 maximum SCE for the entire observation period and area (Fig. 2) was 2 %, 43 %, and 74 %, respectively.  
265 SCE showed the presence of a clear linear relationship with elevation (coefficient of  
266 determination ( $r^2$ ) = 0.95,  $p < 0.01$ ; Fig. 2d). However, the relationship was imperfect ( $r^2 = 0.34$ ) above  
267 4,000 m a.s.l. due to increased scattering in the accumulation zone of the glaciers. At its maximum, SCE  
268 covered 1,730 km<sup>2</sup> (74%) of the study area, only being present at elevations above 1,250 m a.s.l. SCE  
269 area was normally distributed with highest concentration of SCE observed between 3,250 and 4,000 m  
270 a.s.l. (Fig. 2e). SCE was on average ~11 % less on the eastern side of the Cordillera compared to the  
271 west (Fig. 2a-c).

272



273

274 Figure 2: a) Median snow extent; b) maximum snow cover extent; c) minimum snow cover extent for  
 275 the 16 snow seasons observed (2000–2016) (glaciers are delineated by black); d) Mean SCE change  
 276 with elevation; and e) Snow covered area distribution with elevation.

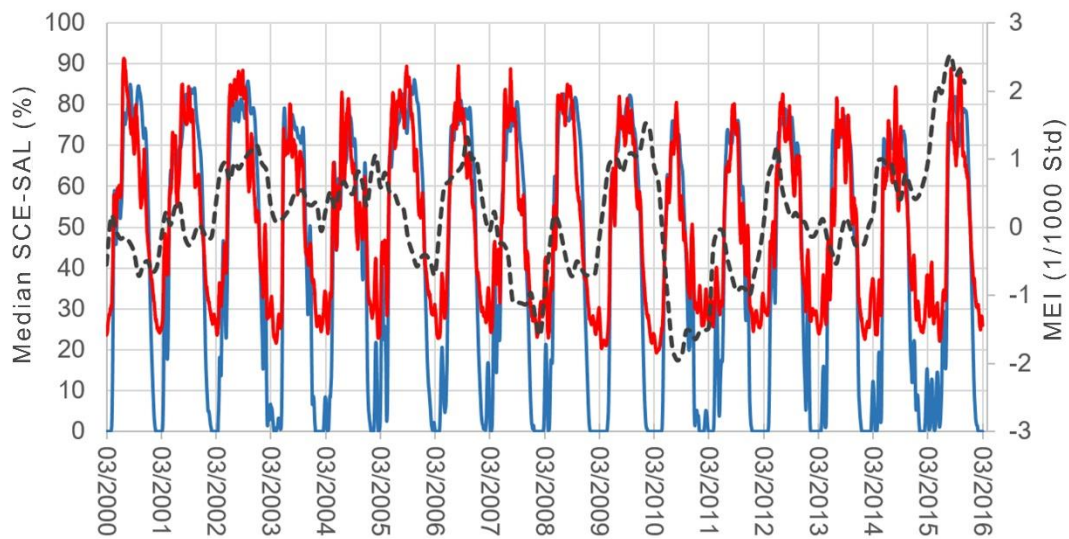
277

278 *5.2 Inter- and intra-annual variability in snow cover extent (SCE) and snow albedo (SAL)*

279

280 The mean SCE over the study area between 2000 and 2016 was approximately ~25 % in austral  
 281 summer and ~68 % in austral winter, reaching a maximum between July 24<sup>th</sup> and 25<sup>th</sup> October and a  
 282 minimum in autumn between March 6<sup>th</sup> and June 6<sup>th</sup> (Fig. 3). Overall, spatial trends for SCE and SAL  
 283 showed widespread downward tendencies (Fig. 4). For SCE, downward trends dominated, with  
 284 medium SCE decreasing by  $13.4 \pm 4.0$  % between 2000 and 2016 ( $0.35$  %  $\text{yr}^{-1}$ ). Demonstrating spatial  
 285 variabilities, the downward trends in SCE were found to be more pronounced for the the eastern side of  
 286 the Cordillera ( $13.9 \pm 4.0$  %,  $0.9$  %  $\text{yr}^{-1}$ ) compared to the west ( $12.4 \pm 3.1$  %,  $0.8$  %  $\text{yr}^{-1}$ ). The eastern side  
 287 of the Cordillera also showed lower SCE but higher SCE variability compared to the western side, this  
 288 despite the eastern side being more elevated (mean elevation for the western and eastern sides is 3,115  
 289 m a.s.l and 3,720 m a.s.l, respectively) (Fig. 2d). Median SAL trends from March 2000 to February  
 290 2016 were also downward with mean values decreasing by  $7.4 \pm 2.2$  % ( $0.5$  %  $\text{yr}^{-1}$ ). Downward trends in  
 291 SAL were shown to be more widespread in the southern parts of the study area compared to northern  
 292 parts. However, we found no significant differences between the eastern and western sides of the  
 293 Cordillera.

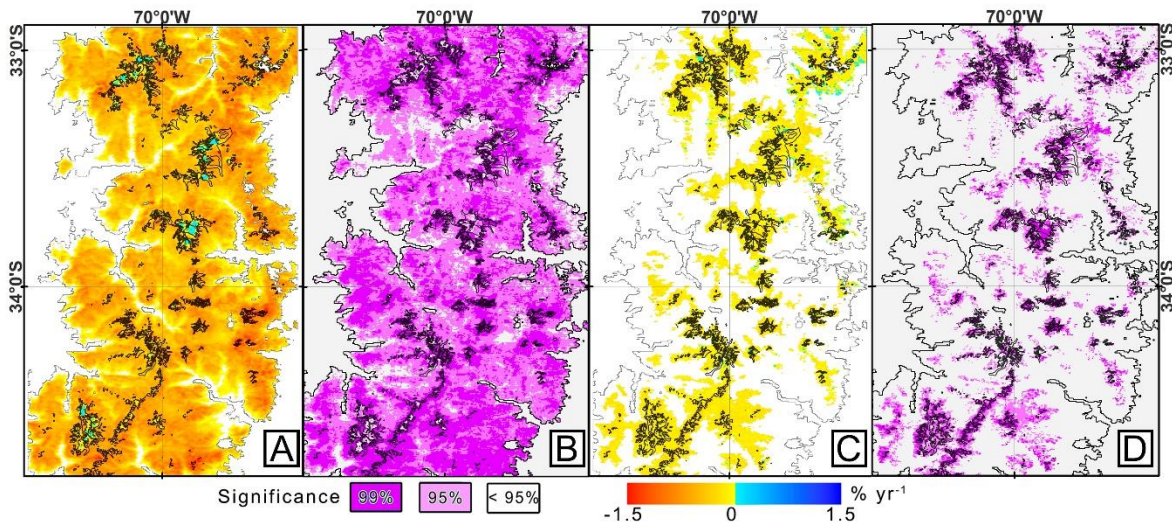
294



295

296 Figure 3: Variation in daily median SCE (blue) and median SAL (red) percentage and the bi-monthly  
 297 multivariate ENSO index (MEI) (dark dashed line) in 1/1000 standard variations (Wolter and Timlin  
 298 2011).

299



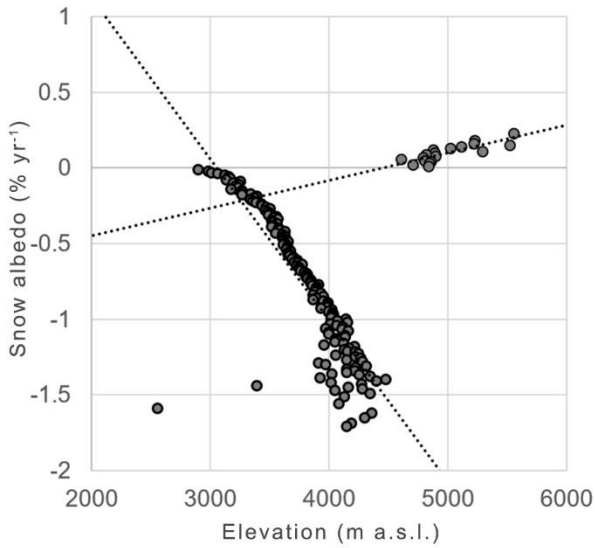
300

301 Figure 4: Linear median trend ( $p < 0.05$ ) in: SCE (a) and SAL (c) from Mar 2000 through Feb 2016, and  
 302 the corresponding significance level of each trend (b, d).

303

304 Comparisons with SRTM data, the SAL trends observed showed negative correlations below  $\sim 4,600$  m  
 305 a.s.l. ( $-1.1 \pm 0.8$  %  $\text{yr}^{-1}$ ,  $r=0.84$ ,  $p < 0.01$ ). Above  $\sim 4,600$  m a.s.l., however, a distinct shift is observed,  
 306 with increasing correlations as a function of elevation ( $0.2 \pm 0.01$  %  $\text{yr}^{-1}$ ,  $r=0.83$ ,  $p < 0.01$ ) (Fig. 5). In  
 307 regards to intra-annual variability, SCE showed pronounced downward trends ( $< -1$  %  $\text{yr}^{-1}$ ) during the  
 308 onset (April, May, and June) and offset (October, November, December, and January) of the snowy  
 309 season. In comparison to SCE, SAL showed slightly less intra-annual variability with most downward  
 310 trends occurring during the onset of the snowy season (Fig. 6).

311

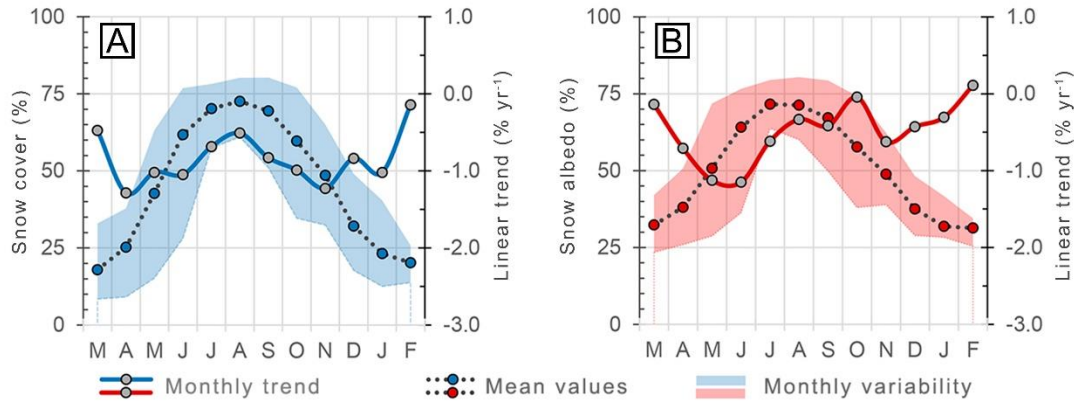


312

313 Figure 5: Trends in snow albedo (SAL) with elevation.

314

315



316

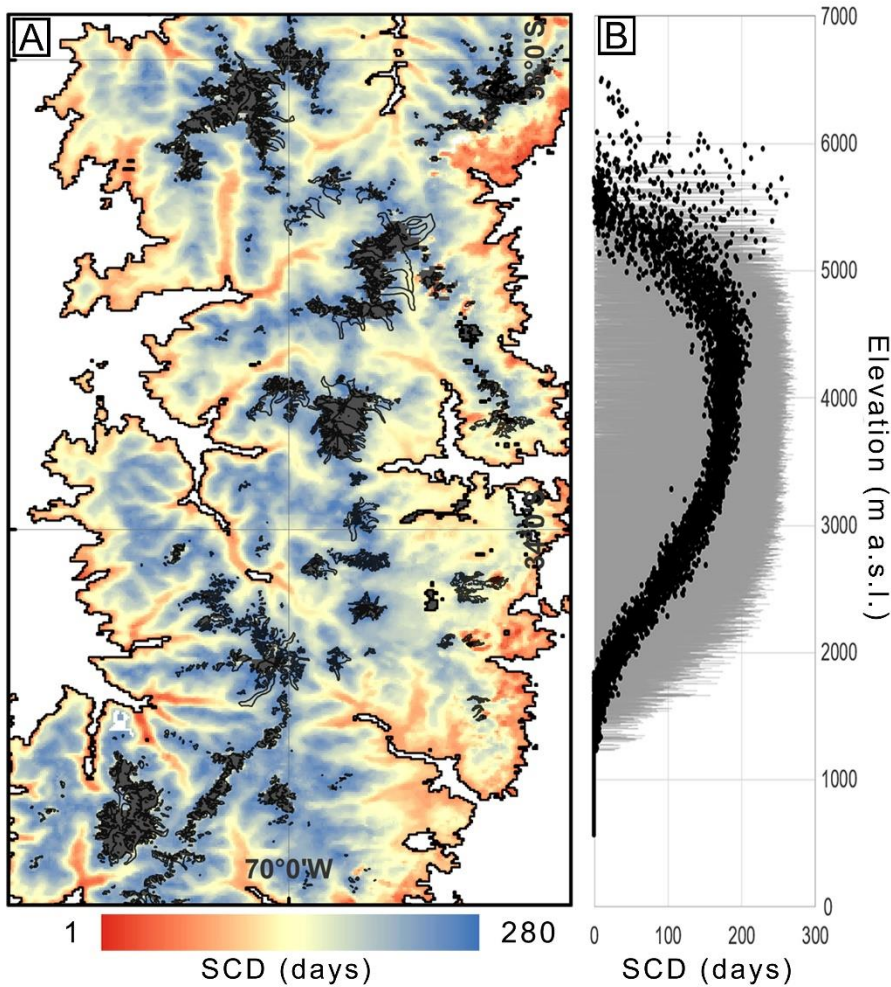
317 Figure 6: Intra-annual linear trends (blue and red lines), monthly mean values (dotted lines) and spread  
 318 (colored areas; monthly minimum and maximum values)) in: (a) snow cover extent (SCE); and (b)  
 319 snow albedo (SAL) between 2000 and 2016.

320

321 *5.3 Snow cover duration (SCD) and seasonal snow cover integral (SCI)*

322 The seasonal SCD values ranged between 0 and 280 days and the seasonal mean SCD ranged  
 323 between 203 days in the 2005–2006 to 130 days in 2011–2012, with an overall median of 173 days  
 324 (Fig. 7a). We observed a strong correlation between SCD and elevation (excluding glacier areas). SCD,  
 325 for example was shown to increase by an average of ~6 days for every 100-meter increment within the

326 2,000 to 4,600 m a.s.l. elevation range ( $r^2=0.80$ ,  $p<0.01$ ) (Fig. 7a). Overall, the trends in SCD were  
 327 downward, showing a mean reduction of  $43 \pm 20$  days for the study period ( $-2.7 \pm 1.3$  days  $\text{yr}^{-1}$ ) (Fig.  
 328 8a). Trends were especially negative on the eastern side of the Cordillera, with a reduction of  $52 \pm 36$   
 329 days ( $3.3 \pm 2.3$  days  $\text{yr}^{-1}$ ), whereas on the western side SCD reduced by  $35 \pm 33$  days ( $2.2 \pm 2.0$  days  $\text{yr}^{-1}$ ).  
 330  
 331



332  
 333 Figure 7: a) Median snow cover duration (SCD, days) 2000–2016 (dark grey areas represent locations  
 334 where the model failed to determine seasonality); and (b) Mean snow cover duration with elevation for  
 335 the 2000–2016 period (grey bars show the spread between minimum and maximum values of SCD as a  
 336 function of elevation).  
 337



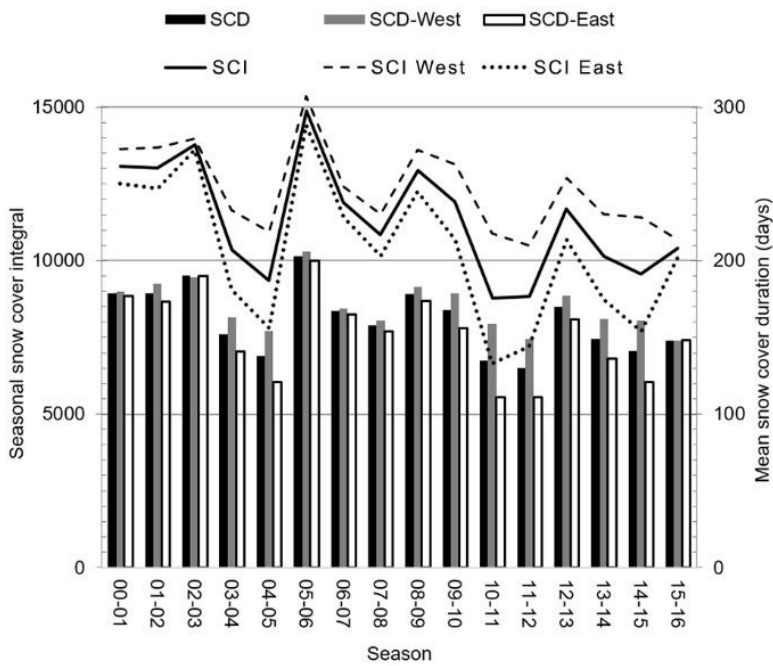
338

339 Figure 8: (a) Per pixel yearly snow cover duration (SCD) trend 2000–2016, and (b) corresponding  
340 significance of trend. Dark gray masked areas represent the mask where SCD values are erroneous and  
341 black lines represent glaciers.

342

343 The SCI for the entire study area declined by  $1.5 \pm 0.5 \text{ \% yr}^{-1}$  (median trend), corresponding to  $25 \pm 8$   
344 % during the full period of 16 snow seasons. The SCI also shows substantial inter-annual variation  
345 (Fig. 9), especially on the eastern side of the Cordillera, where SCI is on average 17 % smaller and  
346 trends are substantially more downward ( $1.8 \pm 0.5 \text{ \% yr}^{-1}$ ) than for the western side ( $1.2 \pm 0.4 \text{ \% yr}^{-1}$ ).

347



348

349 Figure 9: Mean snow cover duration (SCD, bars) and seasonal snow cover integral (SCI, lines) for the  
350 entire study area and for the western (SCD-W) and eastern (SCD-E) sides of the cordillera separately.

351

### 352 5.4 Impact of changes in temperature, precipitation, and El Niño Southern Oscillation (ENSO) on snow 353 cover duration and snow albedo

354

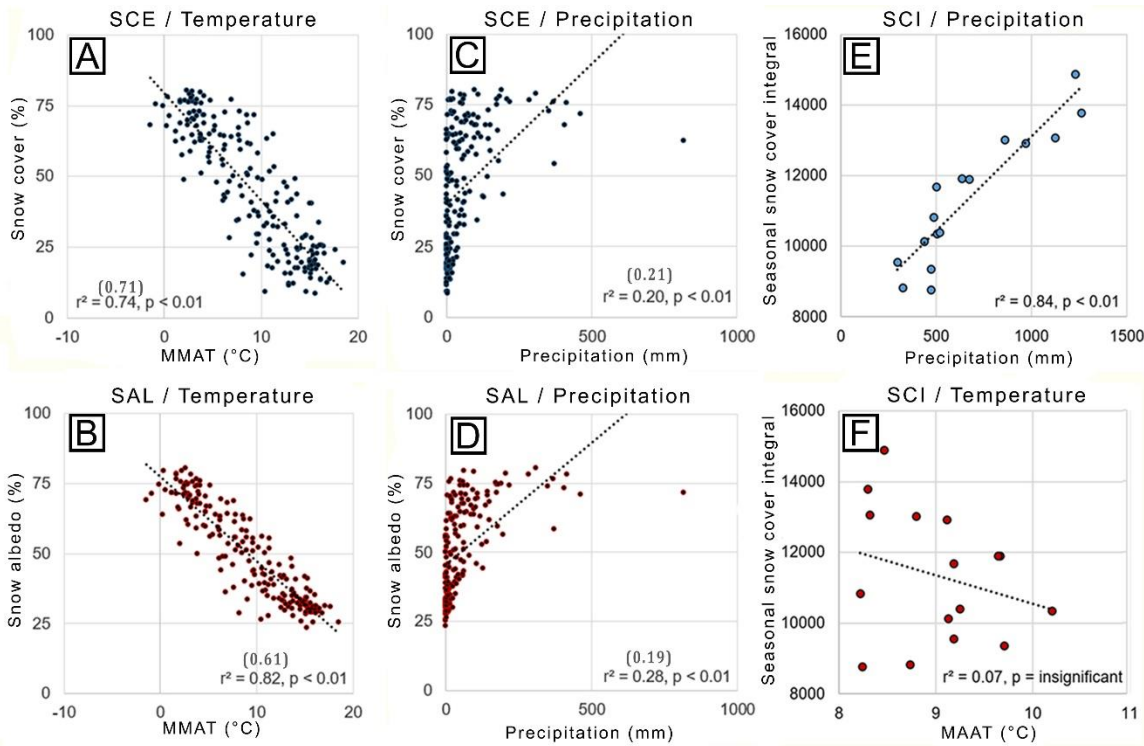
355 Analysis of the meteorological data available from the EYE AWS (Figure 1b) revealed a

significant downward trend in precipitation of  $-4 \text{ mm yr}^{-1}$  and an insignificant trend in MAAT of

356 0.05°C yr<sup>-1</sup> between 2000 and 2016. Between 2000 and 2009, nine extreme precipitation events (>200  
357 mm month<sup>-1</sup>) were identified, with the 2003-2004 season (March-February) receiving a maximum of  
358 1,259 mm. These 'extreme' events occurred mostly during austral winters and account for large  
359 differences in inter-annual precipitation amounts, SCE and SCD sums. Post 2009, no extreme  
360 precipitation events occurred, however a minimum of 317 mm was observed for the 2014-2015 season.  
361 The mean annual precipitation sum for the 2000 to 2016 observation period was 677 mm. MAAT for  
362 this observation period was 9.0°C, with maximum and minimum values of 10.3°C and 7.3°C measured  
363 for the 2003-2004 and 2011-2012 seasons, respectively.

364 Statistical comparisons between the MODIS-derived snow data and the observed EYE  
365 meteorological data revealed that monthly SCE and SAL averaged over the study area and for the pixel  
366 where EYE is located (in brackets) correlated strongly with MMAT ( $r^2$ -values of 0.74 (0.71) and 0.82  
367 (0.61), respectively) (Fig. 10a-b). For the VN met-station, the corresponding comparison between SCE  
368 and MMAT also show a significant correlation for the 2013 to 2016 period ( $r^2$ -values of 0.62). Mean  
369 monthly SCE and SAL also correlate with monthly precipitation sums, but to a lesser extent ( $r^2$ -values  
370 of 0.20 (0.21) and 0.28 (0.19)) (Fig. 10c-d). In comparison, SCI correlated more strongly with annual  
371 precipitation sums ( $r^2$ -value of 0.84) (Fig. 10e).

372



373

374 Figure 10: Relationships between monthly meteorological data (EYE station; Fig. 1) and monthly SCE,  
 375 monthly SAL, and SCI averaged over the study area. a) Monthly SCE against MMAT; b) monthly SAL  
 376 against MMAT, c) Monthly SCE against monthly precipitation sums, d) Monthly SCE against monthly  
 377 precipitation sums, e) SCI against annual precipitation sums, and f) SCI against MAAT.  $r^2$ -values  
 378 between the EYE station data and the pixel where it is located is shown in brackets.

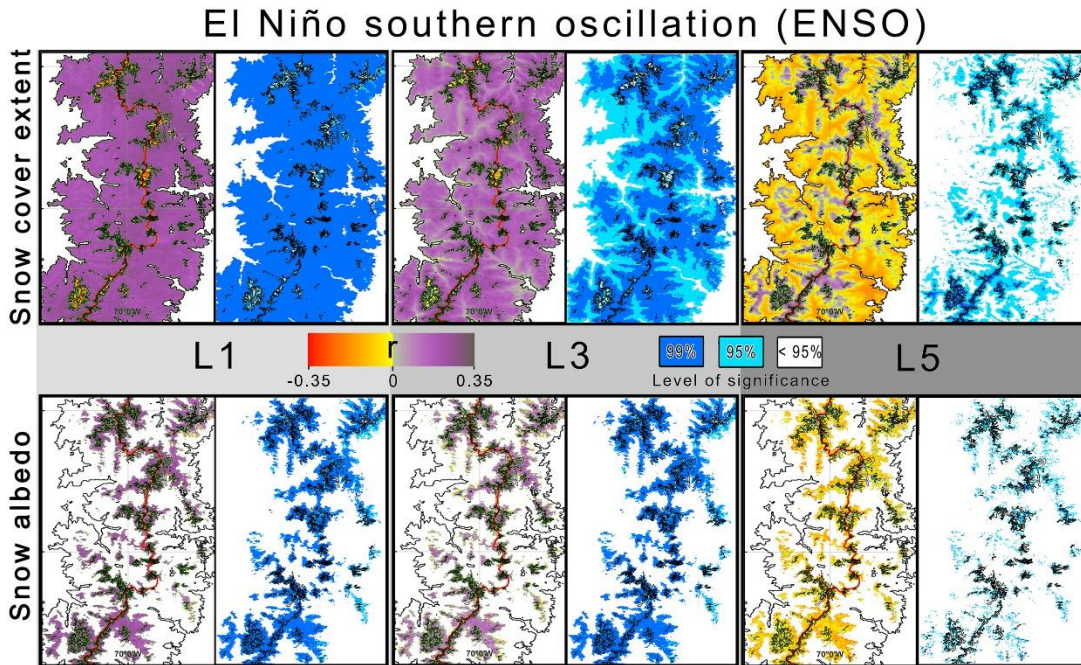
379

380 There can be large uncertainties introduced by comparing a single station with observations  
 381 from a larger study area. However, currently it remains the only long-term continuous dataset available  
 382 in the area, and trends from the local pixel and the station confirms the relationship with trends for the  
 383 area in general (Fig. 10). Furthermore, EYE and NV temperature data significantly correlated ( $r^2$  of  
 384 0.89) showing the temperature trends at EYE and NV being similar at least for that part of the western  
 385 side of the cordillera in the 2013-2016 period.

386

387 ENSO events (MEI) (plotted in Fig. 3) show significant correlations with mean SCE and SAL  
 388 values for the study area (Fig. 11). Mean correlation coefficient values ( $r$ ) between MEI and SCE/SAL  
 389 were strongest when a lag of one month (L1) was applied to the SCE/SAL time series (mean  $r$ -values

390 of 0.21 for the study area). Generally, glaciated areas where snow cover is already present are  
 391 characterized by negative SCE and ENSO correlations for shorter lag periods (L1), which is in contrast  
 392 to the surrounding snow covered areas. This pattern is reversed for longer lag periods (e.g., five  
 393 months), when glaciated and higher elevated areas significantly correlate with ENSO, whereas  
 394 surrounding lower altitude areas are characterized by negative correlations.  
 395



396  
 397 Figure 11: Per-pixel correlations and significance of SCE/SAL with the ENSO index (MEI) including  
 398 one-, three- and five-month lag time (L1, L3, and L5). Red line demarks the east west divide.  
 399

## 400 6. Discussion

### 401 402 6.1 Monitoring and assessment of snow cover and snow albedo

403 Spatio-temporal analysis of MODIS-derived SCE, SAL, SCD, and SCI data revealed significant  
 404 changes during the observation period of this study. Key to the interpretation of these results is the  
 405 quantification of sensor related errors and their influence on the trends observed (2000–2016).  
 406 Unfortunately, only a few validation studies of the MOD10A1 C6 products have been published to  
 407 date. Recent studies using MOD10A1 collection C6 for the Greenland ice sheet however found that

408 v.C6 corrects for the C5 temporal trend bias in dry snow areas and that albedo retrieval accuracy in C6  
409 is substantially improved over C5 (Box et al. 2017; Casey et al. 2017). Therefore, the accuracy of this  
410 product is expected to be better than or at least as good as the C5 product, which has been evaluated in  
411 several previous studies (Tekeli et al. 2005; Hall and Riggs 2007; Gao et al. 2010; Arsenault et al.  
412 2014; Marchane et al. 2015). These studies estimate an overall detection error ranging from ~5 % to  
413 ~48 %, depending on locational properties and type of ‘ground truth’ observations used. In general,  
414 spatially homogeneous locations with flat terrain produces less error than in complex terrain with  
415 mixed surface as being the case for this study (Wang et al. 2014; Burakowski et al. 2015; Moustafa et  
416 al. 2017). By applying a per-pixel temporal change analysis approach in the current study, thereby  
417 avoiding direct inter-comparison of pixels characterized by different slope/aspect, the influence of  
418 topography is expected to be reduced to some degree. This should also be seen in the context of the  
419 latitudinal location of the study area (32°50’– 34°50’ S), characterized by an annual range in solar  
420 zenith angles of 28-60 for MODIS overpass times. This makes the region less prone to influences from  
421 mountain shadowing as compared to complex terrain of higher latitudes of the northern/southern  
422 hemisphere. Snow detection in v.6 is expected to show improvements in comparison to previous  
423 versions especially above 1.300 m a.s.l., where the surface temperature screen used in the product  
424 algorithm (which has previously caused false negatives) has been rolled back leaving fewer gaps in the  
425 data (Hall and Riggs 2016).

426 The smoothed and gap-filled MOD10A1 C6 dataset produced with TIMESAT is assumed to  
427 correctly represent the seasonal snow distribution for the area. Here, only the best quality MOD10A1  
428 C6 observations (by including information available from the QA flags; 0=“best quality”) were used  
429 for the Savitzky-Golay function fitting in TIMESAT. By adjusting the data fitting to the upper  
430 envelope of the daily observations, we ensured that the SCE and SAL values follow rapid changes,  
431 which can occur in snow cover extent and albedo. The TIMESAT model uses local function fitting,  
432 where values before and after in the time series are considered. This local function fitting reduces the  
433 chance of error occurrence in the MOD10A1 observed snow cover (Tekeli et al. 2005). For the upper  
434 ablation zones of glaciers, characterized by limited seasonal variability or year round snow SCE, it is  
435 not possible to accurately assess seasonality variables and thereby SCD. In this case, a glacier mask  
436 was applied based on SCE seasonal variability, in doing so, restricting the SCD analysis to non-

437 glaciated areas (Fig. 7a). Out of 709029144 individual pixel records in the time series 24.2 % were  
438 filled with modeled TIMESAT data.

439         Snow albedo detection in mountainous environments from remotely sensed imagery can contain  
440 large errors when measured on terrain with steep slopes. Validation of satellite or aerial imagery based  
441 data using stationary point albedometers can also be challenging because of pronounced mixed pixel  
442 and geolocation issues (Liang et al. 2005; Sorman et al. 2007; Mernild et al. 2015b; Box et al. 2017).  
443 However, these issues are not likely to have significantly influenced the trends observed in this study as  
444 the MOD10A1 pixels are measured in the same pixel location from year to year in a location where  
445 seasonal variation in solar zenith angle influence is relatively low (annual range between 28-60  
446 degrees) compared to higher latitudes of the northern/southern hemisphere. MOD10A1 snow albedo is  
447 produced only for cloud free pixels with full snow cover (+50 %) indicating that for pixels  
448 characterized by limited full snow cover observations seasonal fitting could have influenced the  
449 accuracy of the TIMESAT generated data.

450

## 451 *6.2 Analysis of climate variables*

452         The analysis of the effect of local scale climatic variability presented in this study made use of  
453 two AWS's EYE and VN in the study area. Indeed, the use of a single or just two AWS's is not ideal  
454 when comparing measurements with the spatially large-scale MOD10A1 dataset. Furthermore, given  
455 the location of the AWS's on the western side of the cordillera and the presence of distinct climatic  
456 gradients (e.g. Mernild et al. 2016a), the data recorded is unlikely to be fully representative of the study  
457 area as a whole. However, this scarce coverage of ground observations reflects the general conditions  
458 for mountainous areas of the Andes and underlines the need for remotely sensed monitoring methods.  
459 Additionally, there is a need for high-resolution gridded meteorological products that work well in  
460 complex terrain. A high-resolution meteorological dynamical model combined with remote sensing  
461 derived products is likely to improve our understanding of the climatic variability impact on snow  
462 cover dynamics. Upward trends in MAAT have higher impact the lower the altitudes (mostly  
463 noticeable in the southern part of the study area) causing changes in onset and offset of snow seasons to  
464 be more sensitive to even small changes in temperature (Fig. 4). Low areas with small slope gradient  
465 show higher sensitivity to upward changes in MAAT in regards to snow accumulation. Especially the  
466 low elevated areas on the eastern side of the cordillera show the effect of increased MAAT.

467 Above 4,600 m a.s.l., SCD shows a considerable increase in variability (Fig. 7b). This however  
468 is not surprising as, in highly elevated zones where SCD can be dependent on localized terrain (slope  
469 and area of topographical shadow) and weather conditions. High wind speeds, for example, often make  
470 it less likely for snow cover to persist in certain areas despite high levels of solid precipitation.

471

### 472 *6.3 Drivers of change on snow cover variables*

473 Studies based on modeling, field measurements and remote sensing have provided insights into  
474 the past, current, and future impacts of climate change on snow conditions and runoff in the Andean  
475 river catchments of central Chile and Argentina (Pellicciotti et al. 2007; Apaloo et al. 2012; Delbart et  
476 al. 2015; Mernild et al. 2015a, 2016a, 2016c; Ragettli et al. 2016). A number of these studies have  
477 predicted that air temperatures in the central Andes will continue to increase. An increase in air  
478 temperature, together with seasonal changes in precipitation patterns, will likely result in a decrease in  
479 the amount of runoff from snow melt and an increase in the amount of runoff from rain (Cai et al.  
480 2014; Mernild et al. 2016a, 2016c; Ragettli et al. 2016). Since the 1970's, precipitation events have  
481 generally become more intense but less frequent in central Chile (Falvey and Garreaud 2007; Garreaud  
482 et al. 2009). The EYE precipitation data, for example, shows a number of intense precipitation events  
483 (above 200 mm m<sup>-1</sup>) during the 2000–2009 period. Interestingly, none of these 'intense' events  
484 occurred during the 2010–2016 period.

485 Per-pixel correlations between SCE/SAL and the Multivariate El Niño index (MEI) show that  
486 MEI has a strong and significant impact on inter-annual SCE/SAL variability in the region (Fig. 11).  
487 Although El Niño events are often associated with increases in precipitation, they can also be  
488 associated with increases in air temperature (Cai et al. 2014) which, together, can have a pronounced  
489 altitude dependent effect on snow cover during spring and autumn. An increase in air temperature, for  
490 example, causes the 0°C isotherm to ascend to higher elevations resulting in a larger proportion of  
491 precipitation falling as rain as opposed to snow. Mernild et al. (2016c) observed this phenomenon for  
492 the Olivares basin (33°12' S; 70°09' W) between 1979 and 2014, where precipitation has been  
493 increasingly falling as rain in recent years. This change in the partitioning of precipitation over  
494 mountainous areas can offset the positive effects of increased precipitation on snow accumulation, with  
495 rainfall often enhancing snow and ice melt rates on glacier surfaces. The significant spatial variation in

496 correlation between MEI and SCE for one-month lag, we suspect is caused by the presence of snow  
497 cover on glaciers giving negative or no correlation on short term but increasing correlations with time.

498 Reduction in SCE in this study has also been studied in modelling studies based on MERRA  
499 satellite data (Mernild et al. 2016b, 2016c) which estimate that snow cover extent in the central Andes  
500 has reduced  $\sim 1.3\%$  per decade 2000–2014 (linear trend, for the b1 window in Fig. 1) (Mernild et al.  
501 2016b). Mernild et al. (2016c) suggest that the largest decreases in snow cover have occurred within  
502 the 3,000–5,000 m a.s.l. elevation range, where more than 70 % of seasonal precipitation falls as snow.  
503 In comparison, the rate of SCE change observed in this study for the same period and area is  
504 significantly higher, with per decade reductions equating to  $\sim 2.8\%$ . This difference between the results  
505 presented here and in Mernild et al. (2016c) may either be an indicator of faster SCE reduction during  
506 the 2000–2016 period or highlight possible SCE overestimations in the MERRA model utilized by the  
507 latter. For other regions of the world snow cover reductions are well documented. In the Arctic, for  
508 example, a general decrease in the amount of snow has been observed between 1999 and 2009, together  
509 with reductions in maximum winter snow water equivalent, a later snow-cover onset in autumn and  
510 earlier snow-free date in spring, and a decreasing snow-cover duration (Liston and Hiemstra 2011).  
511 Indeed a warming trend especially during autumn has been identified at EYE (Burger et al. 2018) and  
512 correspond well with the later onset of snow seasons seen in the area (Fig. 6.).  
513 To sustain all year runoff, rivers of the central Andes rely on substantial contributions from snow and  
514 ice-melt, and river discharge here is strongly linked to snow cover changes (Delbart et al. 2015).  
515 Decreases in SCE at the magnitudes shown in this study has the potential to cause a substantial  
516 redistribution in seasonal runoff for this region, where  $\sim 21\%$  of river runoff originates from snow- and  
517 ice- melt (increasing to  $\sim 85\%$  during dry summers) (Peña and Nazarala 1987; Mernild et al. 2016a).  
518 Glaciers in the central Andes are shrinking and down wasting as a consequence of climate warming and  
519 changes in precipitation patterns (Masiokas et al. 2006; Bodin et al. 2010; Gacitua et al. 2015; Malmros  
520 et al. 2016). Although initially increasing, ice melt runoff will begin to reduce in the future as lowest  
521 elevation land ice disappears. If these ice/snow cover trends continue, runoff conditions will likely  
522 change, especially during spring, dry summers and periods of drought, affecting the future  
523 sustainability of freshwater resources in areas downstream of the central Andes (Peña and Nazarala  
524 1987; Delbart et al. 2015; Saavedra et al. 2016; Carey et al. 2017; López-Moreno et al. 2017). Whether



525 this change in runoff will cause the low lying areas in the catchment to become wetter or drier is  
526 largely determined by local topography (Polk et al. 2017, López-Moreno et al. 2017).

527 Directly influencing the surface energy balance, the downward trends in SAL revealed in this  
528 study (Fig. 4) may possibly result in positive feedbacks in regards to snow and ice melt. This trend of  
529 darkening surfaces, either from reduced snow cover or from enhanced melt conditions, is likely to be  
530 reinforced by increasing air temperatures and decreasing precipitation (e.g., Mernild et al. 2016c).  
531 Another positive feedback could be initiated by the accumulation of dust and debris on glacier surfaces  
532 leading to more energy being absorbed and further melt conditions, especially on lower parts of  
533 glaciers (Hansen and Nazarenko 2004; Oerlemans et al. 2009; Arenson et al. 2015). Minimum glacier-  
534 wide albedo has shown to be a good predictor for glacier mass balances conditions for temperate  
535 glaciers (López-Moreno et al. 2017; Polk et al. 2017), which suggests that glaciers in the study area  
536 may have positive mass balances, at least for some of the years analyzed. Decreases in surface albedo  
537 have also been observed for many other glaciated parts of the world (Box et al. 2012; Tedesco et al.  
538 2013; Abermann et al. 2014; Fausto et al. 2015; Mernild et al. 2015b). The mean albedo for the  
539 Greenland ice sheet ablation area (June–August), for example, declined by 22.9 % from 2000 to 2016  
540 while dry snow areas only decreased by 1.2 % (Box et al. 2017). Increasing albedo values seen above  
541 4.600 m a.s.l. (Fig. 5.) are likely contributed to by the increase in precipitation and the presence of dry  
542 snow conditions at high altitudes (Box et al. 2017).

543 The central Andes are dominated by two distinctly different climate systems. On the western  
544 side of the Cordillera the climate is influenced by oceanic atmospheric interactions, whereas on the  
545 eastern side the climate can be considered continental in type (Prohaska 1976). This difference in  
546 climate is highlighted in this study by the relatively weak correlation between SCE/SAL and MEI on  
547 the eastern side of the Cordillera compared to the west. A higher inter-annual variability in SCE and  
548 SCI and more downward trend on the eastern part may be contributed to continental climate conditions  
549 (Fig. 9) as also observed in Saavedra et al. 2017.

550

## 551 **7. Conclusions and outlook**

552 Overall, snow cover extent (SCE) and snow albedo (SAL) decreased by  $13.4 \pm 4$  % and  $7.4 \pm 2$   
553 %, respectively, between 2000 and 2016. SCE showed more downward trends on the eastern side of the  
554 Andes Cordillera ( $13.9 \pm 4$  %), while SAL showed a uniform decline throughout the area. A seasonal

555 analysis revealed downward trends in SCE and SAL for all months of the year, with the largest  
556 decreases occurring during the onset (for SCE and SAL) and at the end of the snow seasons (for SCE)  
557 ( $> 1\% \text{ yr}^{-1}$ ). SCE showed a near linear increase with elevation ( $r^2=0.96, p < 0.01$ ), and largest relative  
558 losses occurring at elevations above 4.600 m a.s.l. outside glaciated areas. Spatial analysis of the SAL  
559 data revealed increasingly downward trends up to  $\sim 4,600$  m a.s.l. in elevation. Above  $\sim 4,600$  m a.s.l.  
560 this trend is reversed, likely because of permanent or semi-permanent dry snow conditions present in  
561 glacier accumulation zone. Snow cover duration (SCD) decreased on average by  $43 \pm 20$  days  
562 throughout the study area between 2000 and 2016 with largest changes occurring at elevations below  
563 4.500 m a.s.l. on the eastern side and 3.500 m a.s.l. on the western side.

564 TIMESAT was unable to extract SCD for glacier areas that were covered with snow for most of  
565 the year due to the lack of seasonal variation. Additionally, in situations of large variations in snow  
566 conditions occurring over a very short time period the Savitzky-Golay seasonal fitting process applied  
567 may introduce some errors. SCD trends for the study area indicate a shortening of the snow season  
568 between 2000 and 2016. SCI trends for the included glacial areas were also shown to be downward  
569 during this 16-year observation period (these being more pronounced on the eastern side of the  
570 Cordillera).

571 The impact of ENSO events, which influence largescale precipitation and temperature patterns  
572 in the study area, on the SCE, SCD, and SAL was shown to be evident. Per-pixel analyses revealed that  
573 ENSO positively influences SCE/SAL values most strongly with a one-month time-lag. Data available  
574 from the EYE meteorological station, between 2000 and 2016, reveals that the monthly SCE and SAL  
575 values are primarily determined by variations in temperature, whilst montly SCI values are determined  
576 mostly by precipitation. If the observed decline in SCE persist in the coming years, it will likely result  
577 in a seasonal redistribution of available downstream freshwater which may cause future problems for  
578 people and agriculture in the region.

579

## 580 **Acknowledgements**

581 We extend a special thanks to the editor and the reviewers for their insightful critique of this  
582 article. This work was supported by the Chilean Fondecyt Regular Competition under grant agreement  
583 #1140172. All data requests should be addressed to the first author. The authors have no conflict of  
584 interest.

585

586

587 **References:**

- 588 Abermann, J., Kinnard, C., & MacDonell, S. (2014). Albedo variations and the impact of clouds on  
589 glaciers in the Chilean semi-arid Andes. *Journal of Glaciology*, 60, 183-191
- 590 Apaloo, J., Brenning, A., & Bodin, X. (2012). Interactions between Seasonal Snow Cover, Ground  
591 Surface Temperature and Topography (Andes of Santiago, Chile, 33.5°S). *Permafrost and*  
592 *Periglacial Processes*, 23, 277-291
- 593 Arenson, L.U., Jakob, M., & Wainstein, P. (2015). Effects of Dust Deposition on Glacier Ablation and  
594 Runoff at the Pascua-Lama Mining Project, Chile and Argentina. In G. Lollino, A. Manconi, J.  
595 Clague, W. Shan, & M. Chiarle (Eds.), *Engineering Geology for Society and Territory - Volume*  
596 *1: Climate Change and Engineering Geology* (pp. 27-32). Cham: Springer International  
597 Publishing
- 598 Arsenault, K.R., Houser, P.R., & De Lannoy, G.J.M. (2014). Evaluation of the MODIS snow cover  
599 fraction product. *Hydrological Processes*, 28, 980-998
- 600 Benn, D.I., & Evans, D.J.A. (2010). *Glaciers and glaciation*. London: Hodder Education
- 601 Bodin, X., Rojas, F., & Brenning, A. (2010). Status and evolution of the cryosphere in the Andes of  
602 Santiago (Chile, 33.5 degrees S.). *Geomorphology*, 118, 453-464
- 603 Box, J.E., Fettweis, X., Stroeve, J.C., Tedesco, M., Hall, D.K., & Steffen, K. (2012). Greenland ice  
604 sheet albedo feedback: thermodynamics and atmospheric drivers. *The Cryosphere*, 6, 821-839
- 605 Box, J.E., Van As, D., Steffen, K., Fausto, R.S., Ahlstrøm, A.P., Citterio, M., & Andersen, S.B. (2017).  
606 Greenland, Canadian and Icelandic land-ice albedo grids (2000–2016). *Geol. Surv. Den.*  
607 *Greenl. Bull*, 38, 53-56
- 608 Brock, B.W., Willis, I.C., & Sharp, M.J. (2000). Measurement and parameterization of albedo  
609 variations at Haut Glacier d'Arolla, Switzerland. *Journal of Glaciology*, 46, 675-688
- 610 Burakowski, E.A., Ollinger, S.V., Lepine, L., Schaaf, C.B., Wang, Z., Dibb, J.E., Hollinger, D.Y., Kim,  
611 J., Erb, A., & Martin, M. (2015). Spatial scaling of reflectance and surface albedo over a mixed-  
612 use, temperate forest landscape during snow-covered periods. *Remote Sensing of Environment*,  
613 158, 465-477

- 614 Burger, F., Brock, B., & Montecinos, A. (2018). Seasonal and elevational contrasts in temperature  
615 trends in Central Chile between 1979 and 2015. *Global and Planetary Change (In Press)*
- 616 Cai, W., Borlace, S., Lengaigne, M., van Rensch, P., Collins, M., Vecchi, G., Timmermann, A.,  
617 Santoso, A., McPhaden, M.J., Wu, L., England, M.H., Wang, G., Guilyardi, E., & Jin, F.-F.  
618 (2014). Increasing frequency of extreme El Nino events due to greenhouse warming. *Nature*  
619 *Clim. Change*, 4, 111-116
- 620 Carey, M., Molden, O.C., Rasmussen, M.B., Jackson, M., Nolin, A.W., & Mark, B.G. (2017). Impacts  
621 of Glacier Recession and Declining Meltwater on Mountain Societies. *Annals of the American*  
622 *Association of Geographers*, 107, 350-359
- 623 Casey, K.A., Polashenski, C.M., Chen, J., & Tedesco, M. (2017). Impact of MODIS sensor calibration  
624 updates on Greenland Ice Sheet surface reflectance and albedo trends. *The Cryosphere*, 11,  
625 1781-1795
- 626 Cereceda-Balic, F., Palomo-Marín, M.R., Bernalte, E., Vidal, V., Christie, J., Fadic,  
627 X., Guevara, J.L., Miro, C., & Pinilla Gil, E. (2012). Impact of Santiago de Chile urban  
628 atmospheric pollution on anthropogenic trace elements enrichment in snow precipitation at  
629 Cerro Colorado, Central Andes. *Atmospheric Environment*, 47, 51-57
- 630 Cornwell, E., Molotch, N.P., & McPhee, J. (2016). Spatio-temporal variability of snow water  
631 equivalent in the extra-tropical Andes Cordillera from distributed energy balance modeling and  
632 remotely sensed snow cover. *Hydrology and Earth System Sciences*, 20, 411-430
- 633 Corripio, J.G., & Purves, R.S. (2006). Surface Energy Balance of High Altitude Glaciers in the Central  
634 Andes: The Effect of Snow Penitentes. *Climate and Hydrology in Mountain Areas* (pp. 15-27):  
635 John Wiley & Sons, Ltd
- 636 Cuffey, K.M., & Paterson, W.S.B. (2010). *The Physics of Glaciers*. Elsevier Science
- 637 Dariane, A.B., Khoramian, A. & Santi, E. (2017). Investigating spatiotemporal snow cover variability  
638 via cloud-free MODIS snow cover product in Central Alborz Region. *Remote Sensing of*  
639 *Environment*, 202, 152-165.
- 640 Delbart, N., Dunesme, S., Lavie, E., Madelin, M., & Goma, R. (2015). Remote sensing of Andean  
641 mountain snow cover to forecast water discharge of Cuyo rivers. *Journal of Alpine Research*,  
642 15
- 643 Dozier, J., & Frew, J. (1981). Atmospheric Corrections to Satellite Radiometric Data over Rugged  
644 Terrain. *Remote Sensing of Environment*, 11, 191-205

644 Dozier, J., Painter, T.H., Rittger, K., & Frew, J.E. (2008). Time-space continuity of daily maps of  
645 fractional snow cover and albedo from MODIS. *Advances in Water Resources*, 31, 1515-1526

646 Dubayah, R. (1992). Estimating Net Solar-Radiation Using Landsat Thematic Mapper and Digital  
647 Elevation Data. *Water Resources Research*, 28, 2469-2484

648 Dumont, M., Gardelle, J., Sirguey, P., Guillot, A., Six, D., Rabatel, A., & Arnaud, Y. (2012). Linking  
649 glacier annual mass balance and glacier albedo retrieved from MODIS data. *The Cryosphere*, 6,  
650 1527-1539

651 Eastman, J.R. (2009). IDRISI Taiga guide to GIS and image processing. *Clark Labs Clark University,*  
652 *Worcester, MA*

653 Eklundh, L., & Jönsson, P. (2015). TIMESAT: A Software Package for Time-Series Processing and  
654 Assessment of Vegetation Dynamics. In C. Kuenzer, S. Dech, & W. Wagner (Eds.), *Remote*  
655 *Sensing Time Series: Revealing Land Surface Dynamics* (pp. 141-158). Cham: Springer  
656 International Publishing

657 Escobar, F., Casassa, G., & Pozo, V. (1995). Variaciones de un glaciar de Montaña en los Andes de  
658 Chile Central en las últimas dos décadas. *Bulletin de l'Institut français d'études andines*, 24,  
659 683-995

660 Falvey, M., & Garreaud, R. (2007). Wintertime Precipitation Episodes in Central Chile: Associated  
661 Meteorological Conditions and Orographic Influences. *Journal of Hydrometeorology*, 8, 171-  
662 193

663 Falvey, M., & Garreaud, R.D. (2009). Regional cooling in a warming world: Recent temperature trends  
664 in the southeast Pacific and along the west coast of subtropical South America (1979-2006).  
665 *Journal of Geophysical Research-Atmospheres*, 114

666 Farr, T.G., Rosen, P.A., Caro, E., Crippen, R., Duren, R., Hensley, S., Kobrick, M., Paller, M.,  
667 Rodriguez, E., Roth, L., Seal, D., Shaffer, S., Shimada, J., Umland, J., Werner, M., Oskin, M.,  
668 Burbank, D., & Alsdorf, D. (2007). The Shuttle Radar Topography Mission. *Reviews of*  
669 *Geophysics*, 45, n/a-n/a

670 Fausto, R.S., van As, D., Antoft, J.A., Box, J.E., Colgan, W., & Team, P.P. (2015). Greenland ice sheet  
671 melt area from MODIS (2000-2014). *Geological Survey of Denmark and Greenland Bulletin*,  
672 57-60

- 673 Gacitua, G., Uribe, J.A., R., W., Loriaux, T., Hernandez, J., & Rivera, A. (2015). 50MHz helicopter-  
674 borne radar data for determination of glacier thermal regime in the central Chilean Andes.  
675 *Annals of Glaciology*, 56
- 676 Gao, Y., Xie, H.J., Yao, T.D., & Xue, C.S. (2010). Integrated assessment on multi-temporal and multi-  
677 sensor combinations for reducing cloud obscuration of MODIS snow cover products of the  
678 Pacific Northwest USA. *Remote Sensing of Environment*, 114, 1662-1675
- 679 Gardner, A.S., & Sharp, M.J. (2010). A review of snow and ice albedo and the development of a new  
680 physically based broadband albedo parameterization. *Journal of Geophysical Research-Earth*  
681 *Surface*, 115
- 682 Garreaud, R.D., Vuille, M., Compagnucci, R., & Marengo, J. (2009). Present-day South American  
683 climate. *Palaeogeography Palaeoclimatology Palaeoecology*, 281, 180-195
- 684 Gurung, D. R., Maharjan, S. B., Shrestha, A. B., Shrestha, M. S., Bajracharya, S. R. and Murthy, M. S.  
685 R. (2017). Climate and topographic controls on snow cover dynamics in the Hindu Kush  
686 Himalaya. *Int. J. Climatol.*, 37: 3873–3882.
- 687 Hall, D.H., & Riggs, G. (2016). MODIS/Terra Snow Cover Daily L3 Global 500m Grid, Version 6. In  
688 National Snow and Ice Data Center (NSIDC) (Ed.). Boulder, Colorado USA: NASA
- 689 Hall, D.K., & Riggs, G.A. (2007). Accuracy assessment of the MODIS snow products. *Hydrological*  
690 *Processes*, 21, 1534-1547
- 691 Hall, D.K., Riggs, G.A., & Salomonson, V.V. (1995). Development of methods for mapping global  
692 snow cover using moderate resolution imaging spectroradiometer data. *Remote Sensing of*  
693 *Environment*, 54, 127-140
- 694 Hall, D.K., Riggs, G.A., Salomonson, V.V., DiGirolamo, N.E., & Bayr, K.J. (2002). MODIS snow-  
695 cover products. *Remote Sensing of Environment*, 83, 181-194
- 696 Hansen, J., & Nazarenko, L. (2004). Soot climate forcing via snow and ice albedos. *Proceedings of the*  
697 *National Academy of Sciences of the United States of America*, 101, 423-428
- 698 Hock, R. (2005). Glacier melt: a review of processes and their modelling. *Progress in Physical*  
699 *Geography*, 29, 362-391
- 700 Huang, X., Deng, J., Wang, W., Feng, Q. & Liang, T. (2017). Impact of climate and elevation on snow  
701 cover using integrated remote sensing snow products in Tibetan Plateau. *Remote Sensing of*  
702 *Environment*, 190, 274-288.

- 703 Jönsson, P., & Eklundh, L. (2002). Seasonality extraction by function fitting to time-series of satellite  
704 sensor data. *Ieee Transactions on Geoscience and Remote Sensing*, *40*, 1824-1832
- 705 Jönsson, P., & Eklundh, L. (2004). TIMESAT - a program for analyzing time-series of satellite sensor  
706 data. *Computers & Geosciences*, *30*, 833-845
- 707 Justice, C.O., Vermote, E., Townshend, J.R.G., Defries, R., Roy, D.P., Hall, D.K., Salomonson, V.V.,  
708 Privette, J.L., Riggs, G., Strahler, A., Lucht, W., Myneni, R.B., Knyazikhin, Y., Running, S.W.,  
709 Nemani, R.R., Wan, Z.M., Huete, A.R., van Leeuwen, W., Wolfe, R.E., Giglio, L., Muller, J.P.,  
710 Lewis, P., & Barnsley, M.J. (1998). The Moderate Resolution Imaging Spectroradiometer  
711 (MODIS): Land remote sensing for global change research. *Ieee Transactions on Geoscience  
712 and Remote Sensing*, *36*, 1228-1249
- 713 Kendall, M.G. (1975). *Rank Correlation Methods*. London: Griffin
- 714 Klein, A.G., & Stroeve, J. (2002a). Development and validation of a snow albedo algorithm for the  
715 MODIS instrument. *Annals of Glaciology*, *Vol 34*, 2002, *34*, 45-52
- 716 Klein, A.G., & Stroeve, J. (2002b). Development and validation of a snow albedo algorithm for the  
717 MODIS instrument. *Annals of Glaciology*, *34*, 45-52
- 718 Knap, W.H., Brock, B.W., Oerlemans, J., & Willis, I.C. (1999). Comparison of Landsat TM-derived  
719 and ground-based albedos of Haut Glacier d'Arolla, Switzerland. *International Journal of  
720 Remote Sensing*, *20*, 3293-3310
- 721 Konzelmann, T., & Ohmura, A. (1995). Radiative Fluxes and Their Impact on the Energy-Balance of  
722 the Greenland Ice-Sheet. *Journal of Glaciology*, *41*, 490-502
- 723 Leiva, J.C. (1999). Recent fluctuations of the Argentinian glaciers. *Global and Planetary Change*, *22*,  
724 169-177
- 725 Li, C., Su, F., Yang, D., Tong, K., Meng, F. and Kan, B. (2017). Spatiotemporal variation of snow  
726 cover over the Tibetan Plateau based on MODIS snow product, 2001–2014. *Int. J. Climatol.*  
727 doi:10.1002/joc.5204
- 728 Li, X., Fu, W., Shen, H., Huang, C. & Zhang, L. (2017). Monitoring snow cover variability (2000–  
729 2014) in the Hengduan Mountains based on cloud-removed MODIS products with an adaptive  
730 spatio-temporal weighted method. *Journal of Hydrology*, *551*, 314-327.
- 731 Liang, S.L., Stroeve, J., & Box, J.E. (2005). Mapping daily snow/ice shortwave broadband albedo from  
732 Moderate Resolution Imaging Spectroradiometer (MODIS): The improved direct retrieval

733 algorithm and validation with Greenland in situ measurement. *Journal of Geophysical*  
734 *Research-Atmospheres*, 110

735 Liston, G.E., & Hiemstra, C.A. (2011). The Changing Cryosphere: Pan-Arctic Snow Trends (1979–  
736 2009). *Journal of Climate*, 24, 5691-5712

737 López-Moreno, J.I., Valero-Garcés, B., Mark, B., Condom, T., Revuelto, J., Azorín-Molina, C., Bazo,  
738 J., Frugone, M., Vicente-Serrano, S.M., & Alejo-Cochachin, J. (2017). Hydrological and  
739 depositional processes associated with recent glacier recession in Yanamarey catchment,  
740 Cordillera Blanca (Peru). *Science of the Total Environment*, 579, 272-282

741 Lyapustin, A., Wang, Y., Xiong, X., Meister, G., Platnick, S., Levy, R., Franz, B., Korkin, S., Hilker,  
742 T., Tucker, J., Hall, F., Sellers, P., Wu, A., & Angal, A. (2014). Scientific impact of MODIS C5  
743 calibration degradation and C6+ improvements. *Atmos. Meas. Tech.*, 7, 4353-4365

744 Male, D.H., & Granger, R.J. (1981). Snow Surface-Energy Exchange. *Water Resources Research*, 17,  
745 609-627

746 Malmros, J.K., Mernild, S.H., Wilson, R., Yde, J.C., & Fensholt, R. (2016). Glacier area changes in the  
747 central Chilean and Argentinean Andes 1955-2013/14. *Journal of Glaciology*, 62, 391-401

748 Mann, H.B. (1945). Nonparametric Tests Against Trend. *Econometrica*, 13, 245-259

749 Marchane, A., Jarlan, L., Hanich, L., Boudhar, A., Gascoin, S., Tavernier, A., Filali, N., Le Page, M.,  
750 Hagolle, O., & Berjamy, B. (2015). Assessment of daily MODIS snow cover products to  
751 monitor snow cover dynamics over the Moroccan Atlas mountain range. *Remote Sensing of*  
752 *Environment*, 160, 72-86

753 Masiokas, M.H., Christie, D.A., Le Quesne, C., Pitte, P., Ruiz, L., Villalba, R., Luckman, B.H.,  
754 Berthier, E., Nussbaumer, S.U., González-Reyes, Á., McPhee, J., & Barcaza, G. (2016).  
755 Reconstructing the annual mass balance of the Echaurren Norte glacier (Central Andes, 33.5° S)  
756 using local and regional hydroclimatic data. *The Cryosphere*, 10, 927-940

757 Masiokas, M.H., Villalba, R., Luckman, B.H., Le Quesne, C., & Aravena, J.C. (2006). Snowpack  
758 variations in the central Andes of Argentina and Chile, 1951-2005: Large-scale atmospheric  
759 influences and implications for water resources in the region. *Journal of Climate*, 19, 6334-  
760 6352

761 McClung, D.M. (2013). The effects of El Niño and La Niña on snow and avalanche patterns in British  
762 Columbia, Canada, and central Chile. *Journal of Glaciology*, 59, 783-792



763 Mernild, S.H., Beckerman, A.P., Yde, J.C., Hanna, E., Malmros, J.K., Wilson, R., & Zemp, M.  
764 (2015a). Mass loss and imbalance of glaciers along the Andes Cordillera to the sub-Antarctic  
765 islands. *Global and Planetary Change*, 133, 109-119

766 Mernild, S. H., Liston, G. E., Hiemstra, C. A., Beckerman, A. P., Yde, J. C., and McPhee, J. (2016b).  
767 The Andes Cordillera. Part IV: Spatiotemporal freshwater runoff distribution to adjacent seas  
768 (1979– 2014). *International Journal of Climatology*, 37(7), 3175–3196

769 Mernild, S. H., Liston, G. E., Hiemstra, C. A., Malmros, J. K., Yde, J. C., and McPhee, J. (2016a). The  
770 Andes Cordillera. Part I: Snow Distribution, Properties, and Trends (1979–2014). *International*  
771 *Journal of Climatology*, 37(4), 1680–1698

772 Mernild, S. H., Liston, G. E., Hiemstra, C. A., Yde, J. C., McPhee, J., and Malmros, J. K. (2016c). The  
773 Andes Cordillera. Part II: Rio Olivares Basin Snow Conditions (1979–2014), Central Chile.  
774 *International Journal of Climatology*, 37(4), 1699–1715.,

775 Mernild, S.H., Liston, G.G., Kane, D.L., Knudsen, N.F., & Hasholt, B. (2008). Snow, runoff, and mass  
776 balance modeling for the entire Mittivakkat Glacier (1998-2006), Ammassalik Island, SE  
777 Greenland. *Geografisk Tidsskrift-Danish Journal of Geography*, 108, 121-136

778 Mernild, S.H., Malmros, J.K., Yde, J.C., Wilson, R., Knudsen, N.T., Hanna, E., Fausto, R.S., & van  
779 As, D. (2015b). Albedo decline on Greenland's Mittivakkat Gletscher in a warming climate.  
780 *International Journal of Climatology*, 35, 2294-2307

781 Meza, F.J., Wilks, D.S., Gurovich, L., & Bambach, N. (2012). Impacts of Climate Change on Irrigated  
782 Agriculture in the Maipo Basin, Chile: Reliability of Water Rights and Changes in the Demand  
783 for Irrigation. *Journal of Water Resources Planning and Management*, 138, 421-430

784 Montecinos, A., & Aceituno, P. (2003). Seasonality of the ENSO-related rainfall variability in central  
785 Chile and associated circulation anomalies. *Journal of Climate*, 16, 281-296

786 Moustafa, S.E., Rennermalm, A.K., Román, M.O., Wang, Z., Schaaf, C.B., Smith, L.C., Koenig, L.S.,  
787 & Erb, A. (2017). Evaluation of satellite remote sensing albedo retrievals over the ablation area  
788 of the southwestern Greenland ice sheet. *Remote Sensing of Environment*, 198, 115-125

789 Oerlemans, J., Giesen, R.H., & Van den Broeke, M.R. (2009). Retreating alpine glaciers: increased  
790 melt rates due to accumulation of dust (Vadret da Morteratsch, Switzerland). *Journal of*  
791 *Glaciology*, 55, 729-736

- 792 Neckel, N., Loibl, D., & Rankl, M. (2017). Recent slowdown and thinning of debris-covered glaciers in  
793 south-eastern Tibet. *Earth and Planetary Science Letters*, 464, 95-102
- 794 Pellicciotti, F., Burlando, P., & Van Vliet, K. (2007). Recent trends in precipitation and streamflow in  
795 the Aconcagua River basin, central Chile Glacier mass balance changes and meltwater  
796 discharge. In, *Foz do Iguaçu*. International Association of Hydrological Sciences: IAHS
- 797 Peña, H., & Nazarala, B. (1987). Snowmelt-Runoff Simulation Model of a Central Chile Andean Basin  
798 with Relevant Orographic Effects. In, *International Association of Hydrological Sciences*  
799 (*IAHS*). Vancouver, Canada: IAHS
- 800 Pfeffer, W.T., Arendt, A.A., Bliss, A., Bolch, T., Cogley, J.G., Gardner, A.S., Hagen, J.-O., Hock, R.,  
801 Kaser, G., Kienholz, C., Miles, E.S., Moholdt, G., Mölg, N., Paul, F., Radi, Valentina, Rastner,  
802 P., Raup, B.H., Rich, J., & Sharp, M.J. (2014). The Randolph Glacier Inventory: a globally  
803 complete inventory of glaciers. *Journal of Glaciology*, 60, 537-552
- 804 Polk, M.H., Young, K.R., Baraer, M., Mark, B.G., McKenzie, J.M., Bury, J., & Carey, M. (2017).  
805 Exploring hydrologic connections between tropical mountain wetlands and glacier recession in  
806 Peru's Cordillera Blanca. *Applied Geography*, 78, 94-103
- 807 Prohaska, F. (1976). The climate of Argentina, Paraguay and Uruguay. In W. Schwerdfeger (Ed.),  
808 *World Survey of Climatology* (pp. 13 - 112). New York: Elsevier
- 809 Ragetti, S., Immerzeel, W.W., & Pellicciotti, F. (2016). Contrasting climate change impact on river  
810 flows from high-altitude catchments in the Himalayan and Andes Mountains. *Proceedings of*  
811 *the National Academy of Sciences of the United States of America*, 113, 9222-9227
- 812 Riggs, G.A., Hall, D.K. & Román, M.O. (2017) Overview of NASA's MODIS and Visible Infrared  
813 Imaging Radiometer Suite (VIIRS) snow-cover Earth System Data Records. *Earth Syst. Sci.*  
814 *Data*, 9, 765-777.
- 815 Rittger, K., Painter, T.H., & Dozier, J. (2013). Assessment of methods for mapping snow cover from  
816 MODIS. *Advances in Water Resources*, 51, 367-380
- 817 Rutllant, J., & Fuenzalida, H. (1991). Synoptic Aspects of the Central Chile Rainfall Variability  
818 Associated with the Southern Oscillation. *International Journal of Climatology*, 11, 63-76
- 819 Saavedra, F.A., Kampf, S.K., Fassnacht, S.R., & Sibold, J.S. (2016). A snow climatology of the Andes  
820 Mountains from MODIS snow cover data. *International Journal of Climatology*

821 Saavedra1, F.A., Kampf, S.k., Fassnacht, S.R., and Sibold, J.S. Changes in Andes Mountains snow  
822 cover from MODIS data 2000-2014. *The Cryosphere Discuss.*, [https://doi.org/10.5194/tc-2017-](https://doi.org/10.5194/tc-2017-72)  
823 72, in review, 2017.

824 Savitzky, A., & Golay, M.J.E. (1964). Smoothing and Differentiation of Data by Simplified Least  
825 Squares Procedures. *Analytical Chemistry*, 36, 1627-1639

826 Sirguey, P., Still, H., Cullen, N.J., Dumont, M., Arnaud, Y., & Conway, J.P. (2016). Reconstructing the  
827 mass balance of Brewster Glacier, New Zealand, using MODIS-derived glacier-wide albedo.  
828 *The Cryosphere*, 10, 2465-2484

829 Sorman, A.U., Akyurek, Z., Sensoy, A., Sorman, A.A., & Tekeli, A.E. (2007). Commentary on  
830 comparison of MODIS snow cover and albedo products with ground observations over the  
831 mountainous terrain of Turkey. *Hydrology and Earth System Sciences*, 11, 1353-1360

832 Tedesco, M., Fettweis, X., Mote, T., Wahr, J., Alexander, P., Box, J.E., & Wouters, B. (2013).  
833 Evidence and analysis of 2012 Greenland records from spaceborne observations, a regional  
834 climate model and reanalysis data. *The Cryosphere*, 7, 615-630

835 Tekeli, A.E., Akyürek, Z., Arda Şorman, A., Şensoy, A., & Ünal Şorman, A. (2005). Using MODIS  
836 snow cover maps in modeling snowmelt runoff process in the eastern part of Turkey. *Remote  
837 Sensing of Environment*, 97, 216-230

838 Vuille, M., Kaser, G., & Juen, I. (2008). Glacier mass balance variability in the Cordillera Blanca, Peru  
839 and its relationship with climate and the large-scale circulation. *Global and Planetary Change*,  
840 62, 14-28

841 Wang, Z., Schaaf, C.B., Strahler, A.H., Chopping, M.J., Román, M.O., Shuai, Y., Woodcock, C.E.,  
842 Hollinger, D.Y., & Fitzjarrald, D.R. (2014). Evaluation of MODIS albedo product (MCD43A)  
843 over grassland, agriculture and forest surface types during dormant and snow-covered periods.  
844 *Remote Sensing of Environment*, 140, 60-77

845 Warren, S.G., & Wiscombe, W.J. (1980). A Model for the Spectral Albedo of Snow. II: Snow  
846 Containing Atmospheric Aerosols. *Journal of the Atmospheric Sciences*, 37, 2734-2745

847 Wilson, R., Mernild, S.H., Malmros, J.K., Bravo, C., & CarriÓN, D. (2016). Surface velocity  
848 fluctuations for Glaciar Universidad, central Chile, between 1967 and 2015. *Journal of  
849 Glaciology*, 62, 847-860

- 850 Wiscombe, W.J., & Warren, S.G. (1980). A Model for the Spectral Albedo of Snow. I: Pure Snow.  
851 *Journal of the Atmospheric Sciences*, 37, 2712-2733
- 852 Wolter, K., & Timlin, M.S. (2011). El Niño/Southern Oscillation behaviour since 1871 as diagnosed in  
853 an extended multivariate ENSO index (MEI.ext). *International Journal of Climatology*, 31,  
854 1074-1087
- 855 Xu, W., Ma, H., Wu, D. & Yuan, W. (2017). Assessment of the Daily Cloud-Free MODIS Snow-Cover  
856 Product for Monitoring the Snow-Cover Phenology over the Qinghai-Tibetan Plateau. *Remote*  
857 *Sensing*, 9, 585.